SLAC – PUB – 4285
March 1987
T/E/I

THE MARK II VERTEX DETECTORS: STATUS AND PROSPECTS*

John A. Jaros

Stanford Linear Accelerator Center
Stanford University
Stanford, California 94305

I. INTRODUCTION

The art of detecting heavy quark and lepton decay vertices among the collision products of e^+e^- interactions has developed rapidly in the past ten years. To date, there have been three generations of detectors employed or under construction for measuring and identifying heavy quark and lepton decays. Figure 1 plots the history of the field since the beginning of the PEP/PETRA era in terms of the impact parameter resolution of the detectors. The large central tracking chambers common to the PEP/PETRA detectors were optimized for momentum resolution and reliable jet reconstruction rather than impact parameter resolution. Even so, the 500 μ resolution typical of these devices was adequate for the first tau[1] and B[2] lifetime measurements. In both cases, the resolution was much larger than the average impact parameter of the decay products ($\sim$ 100 μ), so the success of the measurements depended on isolating the decays of interest on the basis of event topology, kinematics, and lepton identification. This was relatively easy in the e^+e^- environment. Because of the poor resolution, the first measurements were just at the limit of statistical significance. Imperfect knowledge of the resolution function added considerable uncertainty to the systematics of the measurements.

* Work supported by the Department of Energy, contract DE – AC03 – 76SF00515.

Invited talk presented at the INFN Eloisotron Project:
Workshop on Vertex Detectors: State of the Art and Perspectives
September 21–26, 1986, Erice, Italy

DR-0267-4

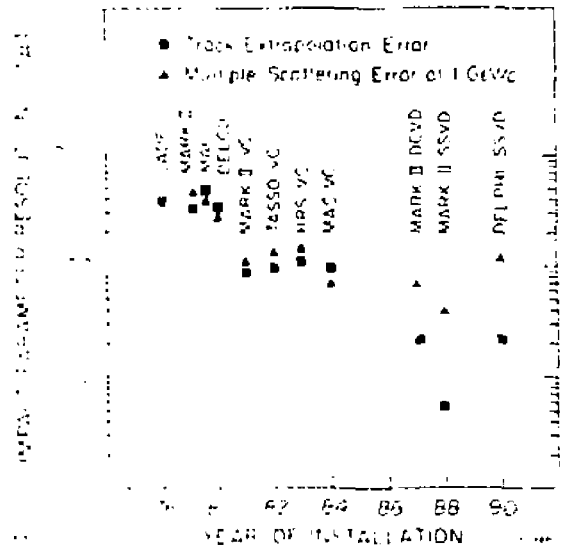

Fig. 1. The impact parameter resolution for existing and proposed collider vertex detectors plotted vs. the year of installation.

The Mark II vertex chamber was the first of the collider "vertex detectors" built expressly for detecting and measuring decay vertices. It boasted sufficient resolution to "detect" a heavy quark decay. The resolution was comparable to the typical impact parameters being measured, resulting in about a $\sqrt{2}$ loss in the statistical precision for lifetime measurements. The Mark II vertex chamber and other second generation detectors have reliably measured the charm, bottom and tau lifetimes, and searched for long-lived anomalies, but they still depend on the cleanliness of the e^+e^- environment to achieve good signal/noise. Decays two or more lifetimes out on the exponential tail can be isolated, so these devices can tag heavy quark jets at low efficiencies. Resolution effects can easily masquerade as physics effects, so a detailed knowledge of the resolution function is required. Despite this limitation several groups[3] have reported τ, B, and D lifetimes with errors below 15%.

Third generation detectors are presently under construction or being planned at TRISTAN, SLC and LEP. They will have impact parameter resolutions significantly smaller than the expected average impact parameters from charm and bottom, and so will measure lifetimes without the loss of statistical precision. The devices will cleanly tag decays that have lived at least one mean lifetime. They will measure lifetimes and KM mixing angles, search for new heavy quarks

and neutrinos, search for the Higgs, and study $B\overline{B}$ oscillations as a function of proper decay time. They will *not* provide an emulsion-like view of the interactions, with its unique association of track to vertex. That will be left to succeeding generations.

This paper will concentrate on the second and third generation Mark II vertex detectors. It will first discuss the Mark II PEP vertex chamber, focusing on our operating experience and our present level of understanding the chamber's performance. Physics results from the chamber are reviewed, and a progress report on a refined measurement of the B lifetime is presented. The rest of the paper is devoted to a technical discussion of the new Mark II Drift Chamber Vertex Detector for the SLC, which is under construction. Chamber design, construction techniques, and prototype performance are discussed. A generation 3+ vertex detector using silicon microstrip detectors is also being built for the Mark II detector, to be used in conjunction with the drift chamber detector. A thorough discussion of this device can be found in Ref. 4.

II. THE MARK II PEP VERTEX CHAMBER

A. Design

The PEP vertex chamber[5] was designed to optimize impact parameter resolution for measurements of heavy quark and lepton lifetimes. The detector consisted of two bands of axial drift cells, the first (four layers deep) at an average radius 11.4 cm from the beams, and the second (three layers deep) at 31.2 cm radius. By measuring points at both small and moderate radii, the chamber permitted track extrapolation to be essentially independent of the less precise central-tracking chamber behind it. To minimize multiple coulomb scattering, the chamber was built directly around a 7.5 cm radius beryllium beam pipe, 0.6% of a radiation length thick including its inner liner of 50 μm titanium which absorbed fluorescence X-rays from nearby synchrotron masks. The chamber was roughly 1.2 m long. The wire load was supported by the outer aluminum shell, which was securely fixed to 2" thick aluminum endplates.

The drift cell was a roughly hexagonal wire structure using 150 μ diameter aluminum field wires. (See Fig. 2.) The exact cell geometry varied cell-to-cell in order to hold the anode-to-field wire distance constant (5.3 mm) throughout the chamber. This had two nice features: (1) tracks (which are essentially radial in the chamber) were always approximately perpendicular to a sense-field layer, so corrections for track angle were unnecessary; (2) a single time-distance relation characterized the entire chamber. The wires were positioned with 15 μm accuracy, so survey and software corrections were unnecessary.

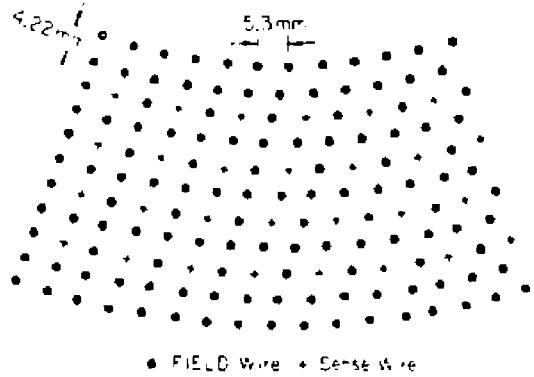

Fig. 2. Arrangement of anode and cathode wires in the Mark II vertex chamber. One-tenth of the four-layer inner band is shown.

The chamber achieved 100 μm resolution per measurement in 1 atm argon/ethane (50/50). This resulted in an impact parameter resolution slightly under 100 μm at high momentum. The multiple coulomb scattering contribution to the impact parameter resolution was 95 μ/P (GeV/c). Roughly 75% of tracks in jet-like multi-hadronic events could be reliably reconstructed and pass tight quality cuts. Losses in efficiency came about when two or more tracks traversed the same drift cell.

B. Operating Experience

The chamber was installed at the PEP storage ring at SLAC in September 1981. Although the pressure vessel was designed for 2 atm operation, leaks associated with the HV feedthroughs, which doubled as pressure feedthroughs, prevented operation at pressures above a few pounds per square inch. Drift velocities in the argon/ethane are sufficiently well saturated that temperature and pressure fluctuations did not affect the time-distance relationship. Prototype tests performed at 2 atm pressure gave improved spatial resolutions ($\sigma \sim 70\ \mu$). However, since multiple scattering errors dominated the impact parameter resolution for most tracks, the fact that we were forced to operate the chamber at 1 atm, with consequently lower resolutions, had very little impact on the physics.

The chamber began routine data taking in November 1981. Anode wires were run at ground potential, the cathode at -2.25 kV, which corresponds to rather high gain on the sense wires. Typical currents were 200 nA/wire in the innermost wires coming primarily from electromagnetic shower spray and beam gas events. During the Spring of 1982, these currents increased to nearly 500 nA/wire as

background levels in PEP increased. After a week or two, one section of the inner band of wires developed "glow discharge" problems, which we assumed were due to Mâlter discharges. The chamber would hold high voltage if the radiation load were low, but would draw large currents and subsequently trip the high voltage supplies in actual beam operations. We lowered the chamber voltage to 1.95 kV in the damaged section (and 2.1 kV elsewhere in the chamber), and added preamplifiers that lowered the threshold sensitivity to about 100 μV, but were forced to run without the damaged section of the chamber in the late spring. The problem wasn't cured until, at the suggestion of M. Atac, we added about 1.6% ethanol to the gas. With the alcohol, it was possible to run the damaged section of the chamber; though we chose to do so at the lower voltages. The chamber operated very reliably during the next two years of data taking. In all, the device logged more than 200 pb^{-1} of data, all at the e^+e^- center of mass energy of 29 GeV.

C. Performance

The Mark II PEP Vertex Chamber resolution is roughly equal to the average impact parameter expected in heavy quark and heavy lepton decays. Thus an observed decay length distribution is the convolution of the primordial exponential distribution with a near-Gaussian resolution function, where the mean decay length is approximately equal to the decay length resolution. A maximum likelihood fit to this distribution has the unfortunate property that the fitted decay length is sensitive to the estimated resolution. So we judged it important to understand the resolution and its possible biases.

The study of the chamber's performance has taken several years and involved many people.[6] Much of the work reported here was done by R. Ong. Three indicators have been used to gauge the performance. The resolution per layer is determined by looking at the cell-by-cell residuals to track fits. Distributions of track χ^2 in the vertex chamber have allowed the global chamber performance to be studied. And the average distance of closest approach to the beam center for Bhabha scattered e^+e^- pairs allows a good check for biases. This is shown in Fig. 3a for an early data set. The figure shows systematic offsets in the one-fifth of the chamber which was run at lowered voltages, and a few isolated offsets with biases in the 50 to 80 μ range. Careful fitting of the time distance relation in the low voltage section, with particular attention to edge effects, eliminated the systematic offsets. A survey of the distribution of residuals (i.e., fitted minus measured drift distance) for all the cells in the chamber, led us to single out a few off-centered and otherwise anomalous distributions. These were corrected by changing time offsets or wire positions, or they were subsequently eliminated from the fits. Figure 3b shows the distance of closest approach distribution after

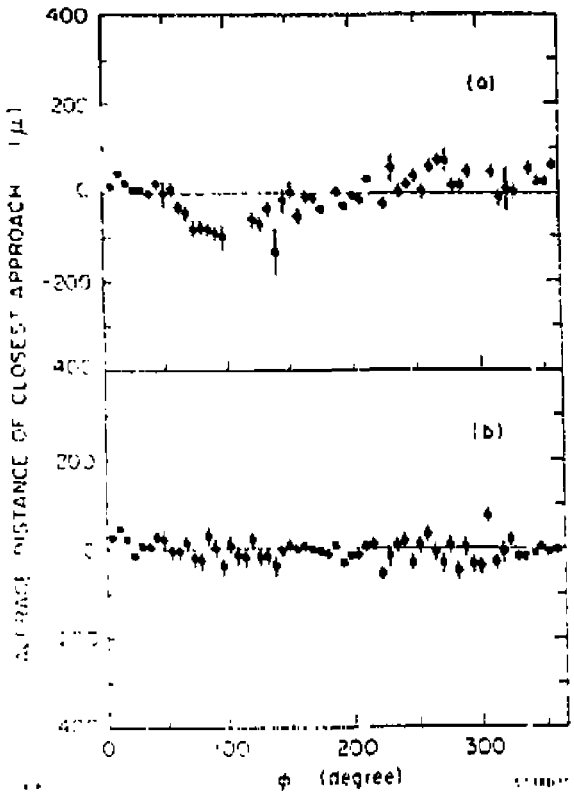

Fig. 3. Average distance of closest approach to the beam center for Bhabha scattered electrons vs. azimuthal angle ϕ. The distribution is shown before (a) and after (b) corrections mentioned in the text.

these fixes, and demonstrates that the remaining systematic biases are at the 40 μ level or below.

Figure 4a shows the vertex chamber track χ^2 distribution for Bhabha tracks, clean, back-to-back events which are easily reconstructed. The curve is the canonical χ^2 distribution for 5 degrees of freedom. Except for an excess of tracks at very large χ^2, the distribution is reasonably well fit, demonstrating that the tracking resolution in the chamber is understood. The resolution is considerably degraded in hadronic events, however, as can be seen from the poor fit in Fig. 4b. This problem is due to cross-talk on the preamplifiers, which skews a given drift time when a neighboring cell has recorded a slightly earlier drift time. After correcting for these nearby hits, the tracking χ^2 distribution is given by Fig. 4c, which shows that even in the hadronic environment the resolution is reasonably well understood.

A final diagnostic is shown in Fig. 5, which shows the distance of separation between two Bhabha tracks after they have been extrapolated to the production

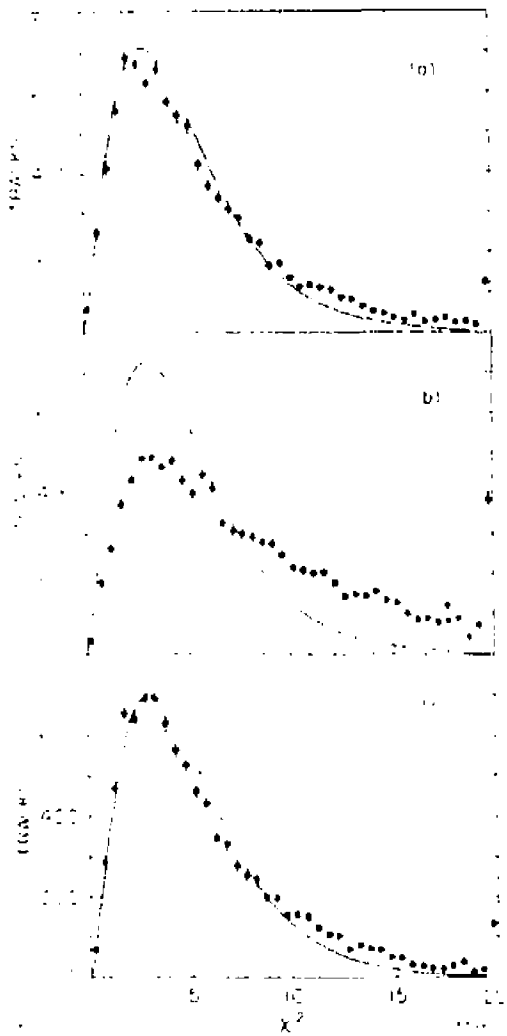

Fig. 4. χ^2 distributions for track fits in the vertex detector for (a) Bhabha scattered electrons, (b) hadronic tracks before cross-talk corrections; (c) hadronic tracks after cross-talk corrections. The solid curve is the canonical χ^2 distribution for five degrees of freedom normalized to the total number of tracks.

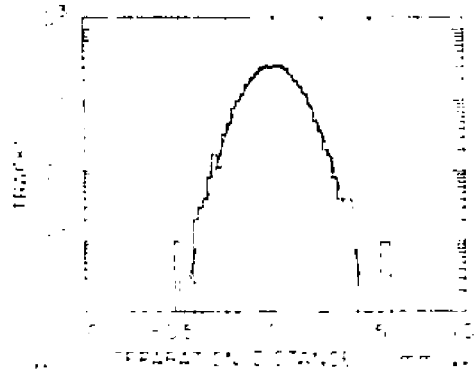

Fig. 5. Projected distance between back-to-back tracks measured in the vicinity of the primary interaction point in Bhabha scattering events. The width of the distribution is 122 μ, implying the impact parameter resolution is 85 μ.

point. The Gaussian curve, which is predicted on the basis of the chamber resolution and the known geometry, correctly describes the observed distribution over several decades, with very little tail. The resolution at the origin is nicely described by a Gaussian of width 85 μ. Similar studies with lower momentum tracks in events of the form $e^+e^- \to e^+e^-\mu^+\mu^-$ and $e^+e^- \to e^+e^-e^+e^-$ have been used to confirm that the multiple scattering contribution to the resolution is 95 μ/P (GeV/c). Impact parameter errors arising from systematic errors in wire placement or momentum errors are negligible in this chamber.

D. Physics Results

The Mark II vertex chamber, and the other detectors of comparable resolution at e^+e^- machines, have produced the first measurements of the tau and bottom hadron lifetimes, confirmed earlier measurements of charmed particle lifetimes, and searched for anomalous decay vertices. Resolution of the second generation devices has not permitted reliable charm tagging, although B tagging at efficiencies of a few percent looks feasible.

The tau lifetime has been measured[7] by isolating a clean sample of tau decays into three charged particles, which is accomplished with simple topological cuts at PEP/PETRA energies. The projected decay length is determined from the known decay vertex and the beam collision point. The tau energy is known (1/2 E_{cm}) and the direction is accurately approximated by the direction of the three-charged-pion system, so the proper lifetime can be deduced. At PEP, the tau decay length averages about 650 μ; the typical measurement

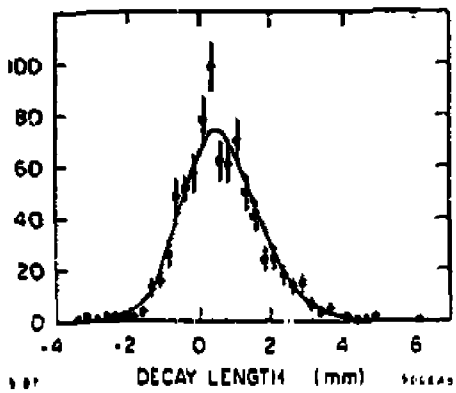

Fig. 6. Decay lengths of tau leptons produced in the reaction $e^+e^- \to \tau^+\tau^-$ at $\sqrt{s} = 29$ GeV.

resolution was 1000 μ. The integrated luminosity of 200 pb^{-1} resulted in about 800 $\tau \to \nu 3\pi(n\pi^0)$ decays, whose decay lengths are plotted in Fig. 6. The measured lifetime was $\tau_\tau = 2.86 \pm 0.16 \pm 0.25 \times 10^{-13}$ sec, in good accord with the theoretical expectation, confirming $e - \mu - \tau$ universality, or in some people's minds, the reliability of a technique with rather modest resolution.

The lifetimes of the D^0 and D^+ mesons have been measured,[8] using much the same technique. The essential step in the measurement was the isolation of a relatively clean sample of mesons. This was accomplished by first identifying D^{*+} mesons (and their charge conjugates). Decays into $D^0\pi^+$ with subsequent D^0 decays into $K^-\pi^+$ and $K^-\pi^+\pi^0$ gave 67 fully reconstructed D^0 mesons. D^{*+} decays into $D^+\pi^0$, with the D^+ decaying into $K^-\pi^+\pi^+$ gave 23 D^+ mesons. Figure 7 shows the measured lifetimes. The observed distributions, which are the convolutions of the exponential decay distributions with our Gaussian-like resolution, are decidedly offset from zero decay length, and just as decidedly nonexponential. The resulting lifetimes, $\tau_{D^0} = 4.7^{+0.9}_{-0.8} \pm 0.5 \times 10^{-13}$ s and $\tau_{D^+} = 8.9^{+3.8}_{-2.7} \pm 1.3 \times 10^{-13}$ s, are in good agreement with other experiments, and overwhelmed by recent advances in statistics and resolution available in fixed target runs.[9]

The discovery[2,10] that the B lifetime is of order 1 picosecond, and not one or two orders of magnitude shorter as had been theoretically expected, underscored the importance of second generation vertex detectors. At PEP and PETRA energies, where the B has sufficient boost to travel a measurable distance, it has so far proved impossible to fully reconstruct B mesons. Instead, experiments have measured the impact parameter of leptons from B semi-leptonic decay, which are

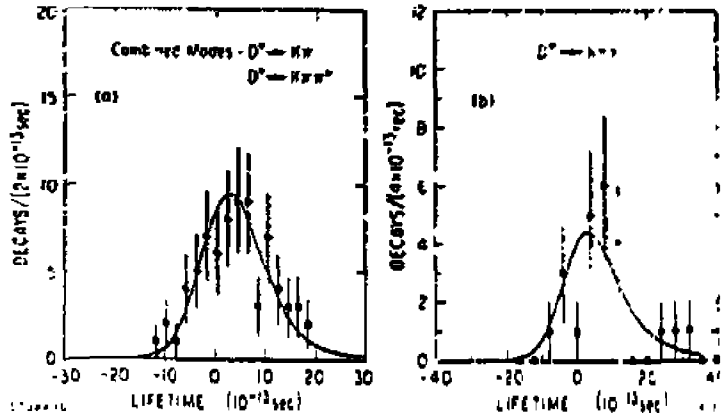

Fig. 7. Proper lifetimes of D^0 and D^+ mesons produced in e^+e^- annihilation at $\sqrt{s} = 29$ GeV.

identified by having large momenta transverse to the hadronic jets in the event. Sample purities are better than 50% B. The impact parameter is measured with respect to the average beam position, as shown in Fig. 8. The impact parameter resolution thus depends on both the track error and the component of the vertical and horizontal beam size perpendicular to the track direction. The large ($\sim$ 400 μ) horizontal beam size dominates the resolution for tracks within about 45° of vertical. Figure 9 shows the distribution of signed impact parameters measured in the Mark II experiment.[11] The B lifetime deduced from the distribution was $0.85 \pm 0.17 \pm 0.21 \times 10^{-12}$ sec. A second technique, with more statistical precision but larger systematic uncertainties was also used.

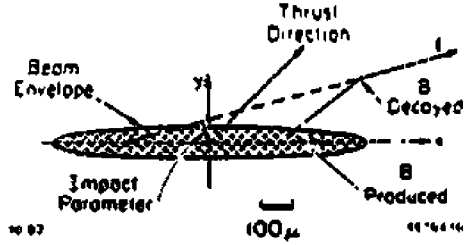

Fig. 8. The projected lepton impact parameter is defined with respect to the average beam position as shown. The thrust direction is used to approximate the B meson direction. The impact parameter is signed positive when the intersection of the lepton direction and the thrust vector corresponds to a positive decay length.

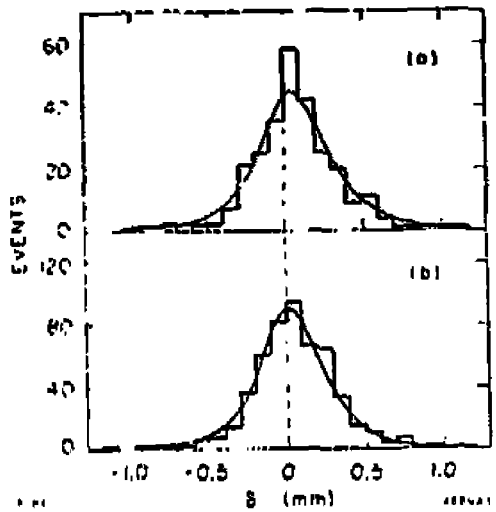

Fig. 9. Lepton impact parameters for (a) high transverse momentum leptons, which come principally from B meson decays; and (b) low transverse momentum leptons, which come primarily from charm decays. The distributions are slightly asymmetric. The mean of the distribution in (a) is 80 ± 17 μ.

We tagged $e^+e^- \to b\bar{b}$ events by selecting events with high transverse momentum leptons, and then vertexed all the well-measured tracks in each jet to form a "jet vertex." Although such a "vertex" contains an admixture of tracks from the primary interaction point, the B decay, and subsequent D decay tracks, the resultant decay length does provide a measure of the B lifetime. Since the B and D decays account for about two-thirds of the charged particles per jet, and for most of the high momentum, and consequently low multiply-scattered and high resolution tracks, B lifetime effects dominate the distribution. Figure 10 shows the jet vertex decay lengths; the resulting B lifetime is $1.25^{+0.26}_{-0.19} \pm 0.50 \times 10^{-12}$ s. Both lifetime determinations are in reasonable agreement with other measurements.[12]

Searches for events with anomalous vertex topologies are in their infancy. We have searched,[13] unsuccessfully, for one class of events with a particularly striking signature. The integrated luminosity at PEP, about 200 pb^{-1}, is sufficient to produce about 70 events of the form $e^+e^- \to \nu\bar{\nu}$ per neutrino generation. We searched for heavy neutrino production, assuming the heavy neutrino would decay sequentially by mixing with the known leptons. The fact that the weak couplings of all leptons are of universal strength argues that the mixing between

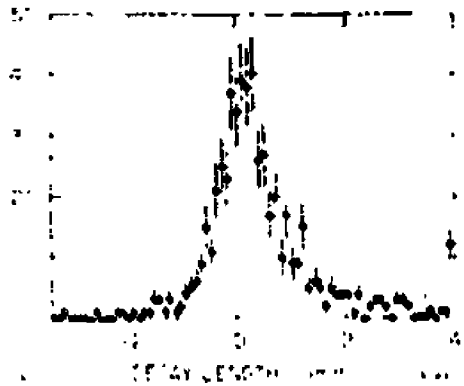

Fig. 10. Jet vertex decay lengths in events with high transverse momentum leptons.

them and any new heavy neutrino are most likely small. Hence the decays might plausibly be inhibited and the resultant decay lengths observable. So we searched for pair-produced objects, one of which decayed between 2 mm and 10 cm of the interaction point in events with no evidence for particle production at the primary interaction point. No events consistent with heavy lepton production were found. Assuming that the heavy neutrino decays like a sequential lepton, and characterizing its coupling to each lepton family in turn by a small Cabibbo-like angle ϵ, the search excludes the existence of heavy neutrinos in certain regions of the mass-mixing angle plane. Figures 11 and 12 show the regions excluded at the 90% Confidence level.

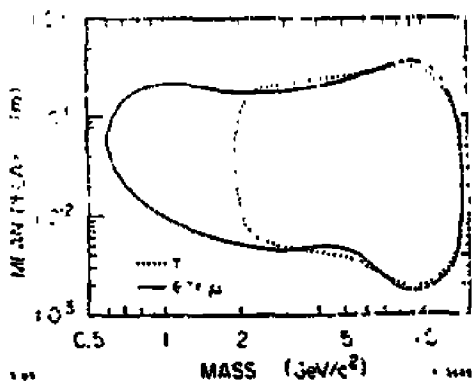

Fig. 11. Heavy neutrinos which mix with e or μ (solid line) or τ (dotted line) are excluded at the 90% confidence level within the contours shown.

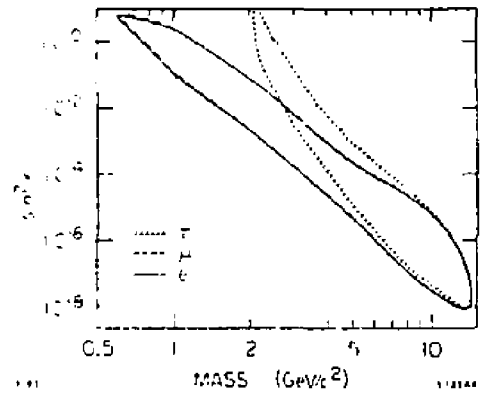

Fig. 12. Excluded regions for heavy neutrinos coupling to e (solid line), μ (dashed line), or τ (dotted line) in terms of the heavy neutrino mass and mixing angle.

A particularly striking event observed in the PEP running is shown in Fig. 13, which shows tracks extrapolated to the vicinity of the primary interaction point, which is indicated by the 1 sigma contour of the beam ellipse. Track number 8 is identified as a muon with 1.1 GeV/c of transverse momentum, tagging the event as a likely example of $e^+e^- \rightarrow b\bar{b}$. Tracks 6, 7, 8, and 14 form a vertex roughly 2 mm from the interaction point. The other tracks in the event group at the opposite end of the beam ellipse. Track 13, having low momentum, has large measurement errors and is compatible with having come from either vertex. The other tracks are measured with roughly 100 μ accuracy. The invariant mass of the tracks which group together in the separated vertex is 4.25 GeV/c^2, well above charm mass, substantiating the hypothesis that this is a long-lived B decay.

E. Update on the B Lifetime Measurement

The measurement of the B lifetime discussed above is being refined by R. Ong of our collaboration. The principal shortcoming of our previous result is that the lepton impact parameter was measured with respect to the average beam position, not the actual production point. As discussed above, this makes the resolution unusually large for vertical tracks. Ong has developed a technique for determining the production point using the other tracks in the event which improves the resolution significantly.

The method is as follows. Each tagged event is divided by a plane perpendicular to the thrust axis to separate particles in one jet from those in the other. A jet

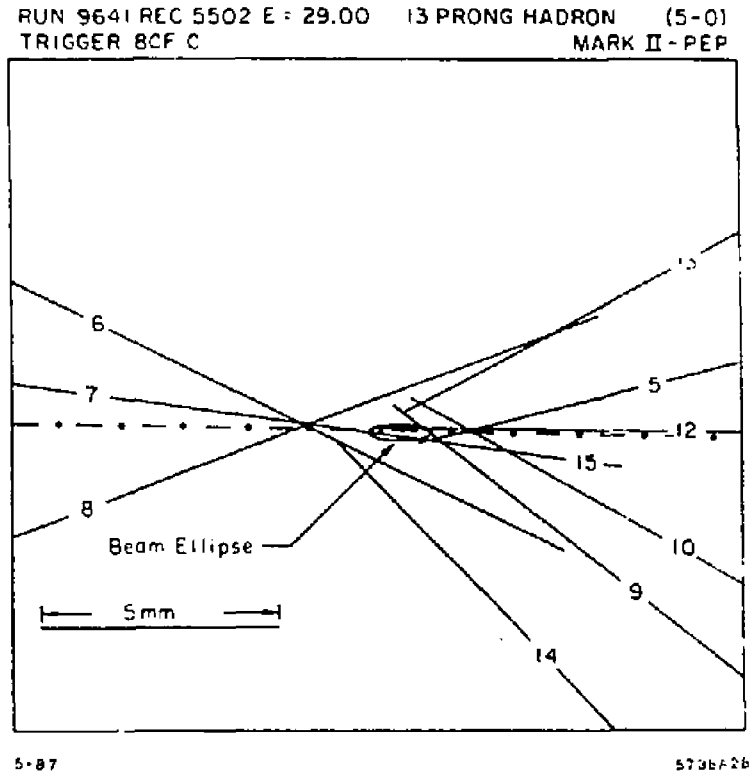

Fig. 13. B decay candidate as seen in the Mark II vertex chamber. The event is described in detail in the text.

vertex is formed from all the well-measured tracks in the jet with momenta above 600 MeV/c, with at least two tracks required for the vertex. The high transverse momentum lepton is included in the vertex. The mean number of tracks in the vertex is 3.6. Of course some of the particles come from the primary interaction point, and some from the B and D decays. Generally speaking, the presence of particles from secondary (or tertiary) decays "pulls" the location of the jet vertex along the B direction, (which is well-approximated by the thrust direction) to a point intermediate between the production and decay points. Pulls transverse to the B direction are small, and average to zero. So to find the production point we take the measured jet vertex, extrapolate back to the beam ellipse along the measured thrust direction, and compute the most likely production point, taking into account the vertex and beam error matrices and uncertainties in the thrust direction. A very thorough simulation with Monte Carlo techniques has shown

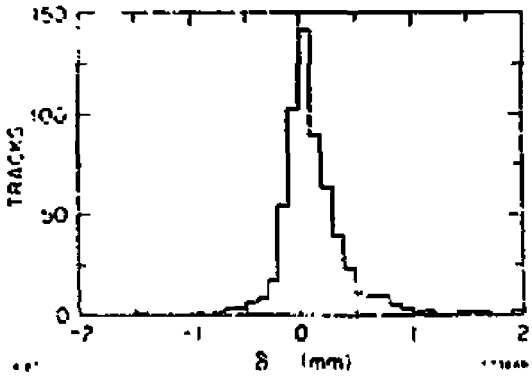

Fig. 14. Lepton impact parameters measured with respect to the primary interaction point.

this estimate of the production point is unbiased for decay lengths below 3 mm, and that the efficiency for finding a jet vertex is constant out to $\leq$ 4 mm decay lengths. The method significantly improves the resolution and roughly doubles the available statistic. Figure 14 shows the resulting impact parameter distribution for leptons. The mean of the distribution is 110 ± 11.9 μ, 9.3 standard deviations from zero. The full analysis of this result is still in progress,[14] and will be reported soon. The resulting B lifetime is close to 1 picosecond.

III. THE MARK II DRIFT CHAMBER VERTEX DETECTOR FOR THE SLC

The Mark II Collaboration is planning to install a drift chamber vertex detector for its 1987 running at the SLC, and to add a microstrip detector to the apparatus the following year. The silicon device is intended to have three layers of detectors, with 12 detectors per layer, and will use 4 microplex readout chips per layer. It is discussed in detail in Ref. 4. The following describes the new drift chamber in some detail.

Figure 15 shows a cut-away drawing of the chamber. It consists of ten pie-shaped jet cells which extend radially between 5 and 17 cm. There are 38 active sense wires in each jet-cell, spaced 2.90 mm apart. The chamber is 55 cm long, and supported by its 1.3 mm thick Beryllium core of radius 4.5 cm, and an outer aluminum shell. It has dual endplates, the first for accurate wire positioning, the second a pressure head. The chamber will operate between 2 and 3 atm pressure with a "slow" gas, i.e., one with unsaturated drift velocity. The drift field will be

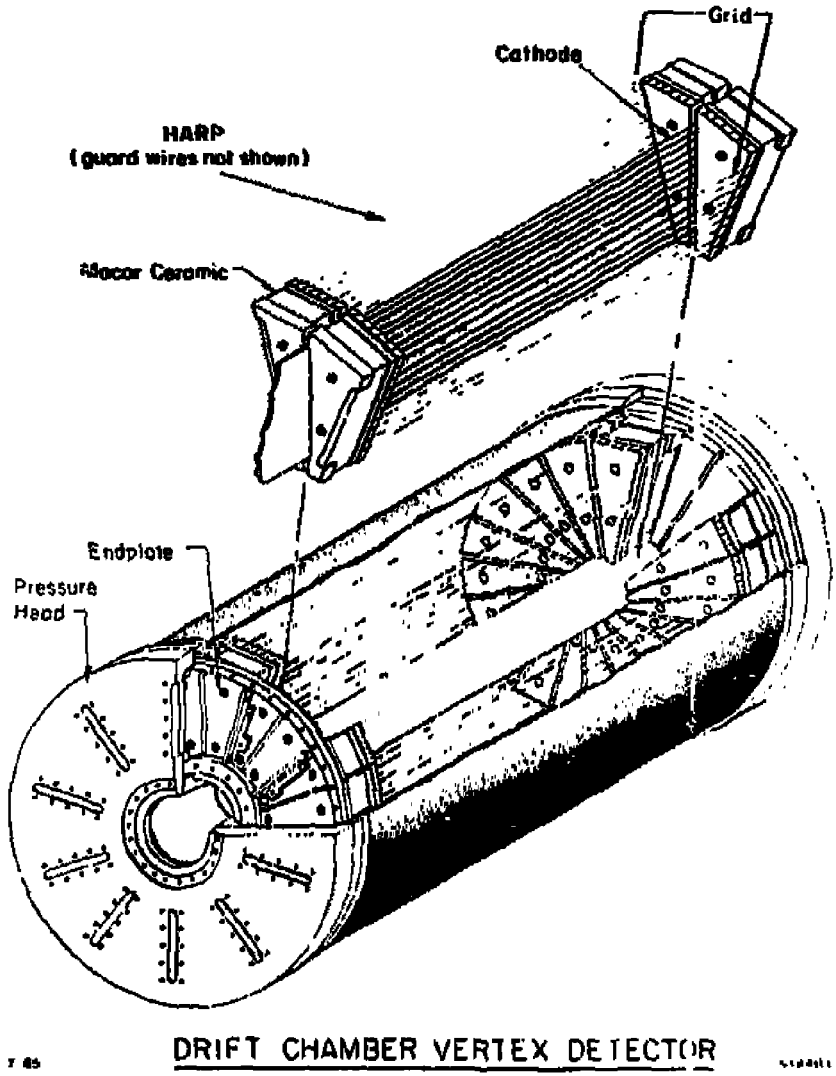

Fig. 15. Cut-away drawing of the Mark II drift chamber vertex detector.

approximately 1 kV/cm atm, and the drift velocity between 5 and 10 μ/ns. The use of a slow gas has several advantages. First, since diffusion remains at the thermal limit in slow gases, the resolution is very good. The accuracy per

measurement will be 30 - 40 μ, averaged over 2 cm of drift. Secondly, since the time between pulses from closely spaced tracks will be more than five times greater than in a fast gas, the electronic problems of resolving such tracks and timing them to the required accuracy become tractable. The principal disadvantage of using slow gases is that the electron drift velocity, and thus the chamber's final calibration, depends on gas composition and density and the magnitude of the electric field. Special care is required to ensure stable chamber operation. The chamber is being constructed by Mark II collaborators from LBL, SLAC, and the University of Colorado, and visitors from KEK.[15]

The SLC environment is ideal for precision vertex detection. The very small beam size will confine the primary interaction to a circle with a radius of a few microns, orders of magnitude smaller than the beam spot in a storage ring. The small beam phase space allows the beam pipe radius to be pushed within 2.5 cm of the beams, thus minimizing the inevitable multiple coulomb scattering. And the repetition rate is sufficiently low that ions can be cleared before the next pulse, eliminating the possibility of space charge effects in the chamber.

A. Cell Design

Our design is a variant of the traditional jet cell,[16] incorporating planes of field shaping wires, called grid planes, on either side of a central plane of alternating anode and potential wires. The design is shown in Fig. 16 along with the field lines. The anode and potential wires are spaced 1.45 mm apart; the grid wires lie directly above the potential wires and are spaced 1.80 mm from them. The anode/potential wire spacing is basically dictated by the desired track-pair resolution. The operating voltages in 3 atm of CO_2/isobutane (92/8) are rather high. The sense wire is held at +3.191 kV, the potential wires at ground, and the grid wires at −0.504 kV. The grid wires serve two functions. They improve the track-pair resolution by "focusing" the electrons onto the anode wire. This minimizes differences in the length of the electron drift trajectories. It also minimizes the variation in field strength, and consequently drift velocity, along the different drift paths. The goal, of course, is isochronous collection. Figure 17 shows the equal-time contours for the cell, plotted on a distance scale appropriate to saturated and unsaturated drift velocities. Ninety-five percent of the charge is collected within about 10 ns in a saturated gas, translating into a track-pair resolution of 500 μ. In an unsaturated gas, the fact that the longest trajectories have the lowest electric fields, worsens this to about 800 μ.

The presence of four independent electrodes (anode, potential wire, grid, and cathode) allows the gain and drift field to be specified, and the cell "tune" to be optimized for isochrony or sense wire electrostatic stability. In practice our

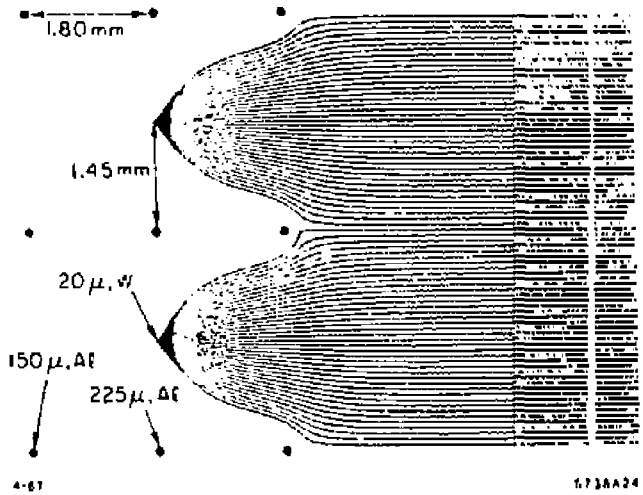

Fig. 16. Detail of the drift cell showing the "focusing" of field lines from the cathode. Tracks which enter the cell are approximately perpendicular to the field lines.

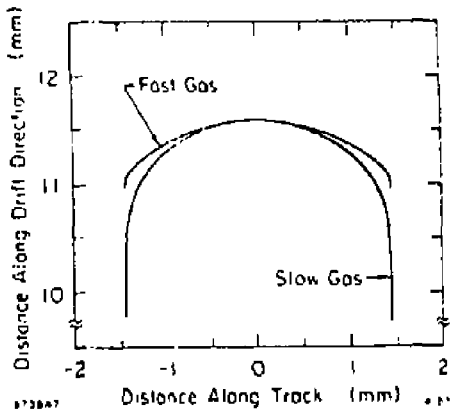

Fig. 17. Electrons deposited along the contours shown are collected isochronously. The offset in the drift distance is arbitrary. The width of the contour is fixed by the sense wire spacing of 2.9 mm.

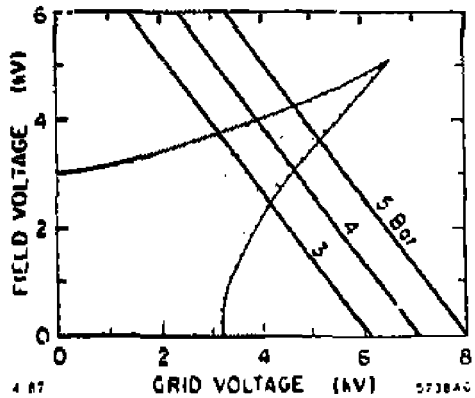

Fig. 18. The sense wire is electrostatically stable for the range of potential wire and grid voltages shown. The chamber operating points in 3, 4, or 5 bar CO_2/C_4H_{10} (92/8) are shown as lines of constant gain.

operating voltages are nearly optimal for both stability and isochrony, so the presence of the grid wires markedly improves the electrostatic stability of the sense wire. Consequently, the chamber could be run at higher gas pressures (with their higher operating voltages), or the wire length could be increased. The range of grid and potential wire voltages (relative to the anode voltage) for which the chamber is stable is shown in Fig. 18.

B. Prototype Results

The performance of this cell has been measured[17] in a prototype chamber with 22 sense wires, the central 8 of which were instrumented. The anode/potential wire spacing was 2.0 mm (not 1.45 mm as in our final chamber), and the cathodes were planar, and 3 cm distant from the grid plane. Resolutions were measured by studying the residuals to straight-line fits through the eight drift cells. All the measurements were made with cosmic rays. Figure 19 shows the observed resolution as a function of drift distance in 3 atm of CO_2/isobutane (92/8) and in argon/ethane (50/50). Drift times were measured by threshold discriminating the outputs of fast amplifiers. The resolutions in the slow gas range from below 20 μ, just outside the grid, to over 40 μ at 2.5 cm drift distance and are proportional to the square root of the drift distance as one expects when diffusion dominates the

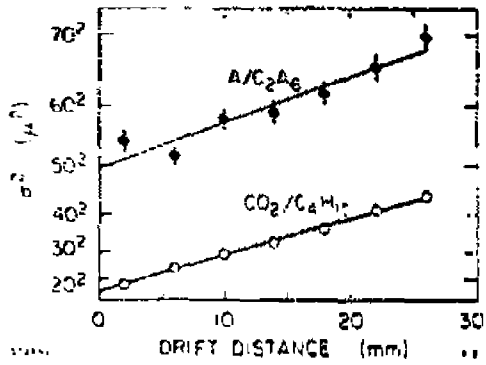

Fig. 19. Resolution squared vs. drift distance at 3 bar pressure in A/C_2H_6 (50/50) and CO_2/C_4H_{10} (92/8) measured in the prototype chamber.

resolution. Surprisingly, the diffusion term in argon/ethane is nearly identical, but the resolution is considerably worse, ranging from 50 to 70 μ.

The resolution, averaged over 2 cm of drift length, is plotted as a function of pressure in Fig. 20. Approximately $\sigma(p) \propto p^{-.7}$. The bulk of this dependence presumably comes from the dependence of the diffusion term on pressure ($\propto p^{-.5}$), the remainder from the improved electron statistics. Figure 21 shows there is little dependence of the average resolution on E/p. In fact, the diffusion contribution decreases as the drift field is increased, but this decrease is compensated by worsening resolution in the grid-anode gap. This result may well be dependent on the type of gas used.

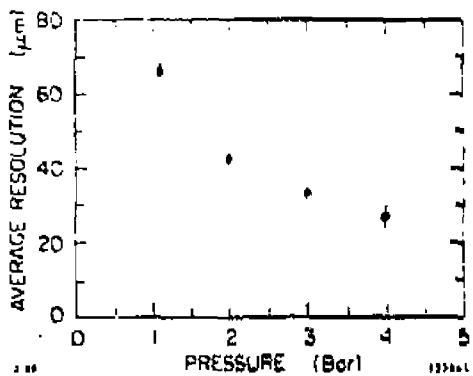

Fig. 20. Dependence of the average resolution on operating pressure.

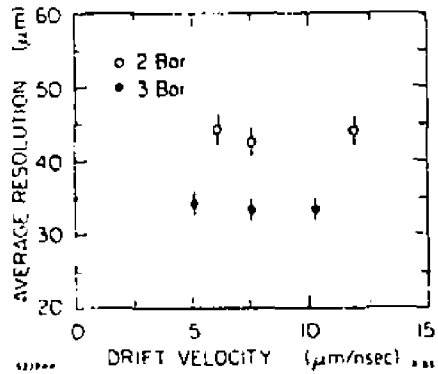

Fig. 21. Dependence of the average resolution on drift velocity at 2 and 3 bar pressures.

Two studies have confirmed that the track-pair resolution is as expected. In the first, we used 100 MHz waveform digitizers to study the average pulse shape for a minimum ionizing particle. It is shown in Fig. 22, where the drift velocity was 7.5 μ/ns. The "error bars" represent the rms of the average pulse height in a single time bin, and show the presence of large fluctuations in the tail of the pulse. Little signal is seen beyond 150 ns, which corresponds to about 1200 μ. The second study used the familiar technique of superposing two independent waveforms at a known separation, and using a simple pattern recognition algorithm to detect the presence of the second peak. Any such algorithm will mistake late arriving ionization in the tail of the first pulse for a second hit;

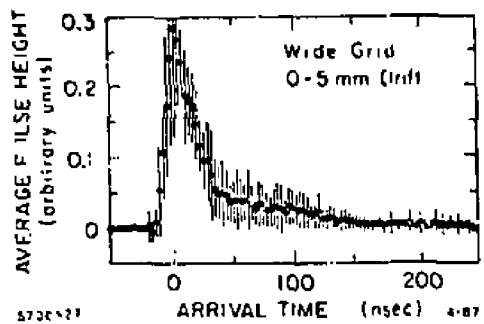

Fig. 22. Average pulse waveform in the prototype chamber at 3 bars pressure. The drift velocity was 7.5 μ/ns. The error bars indicate the root-mean-square of the distribution of pulse heights in any bin.

thus an algorithm has associated with it some "fake rate." Figure 23 shows that a legitimate second pulse is identified with nearly full efficiency beyond 1200 μ in the prototype chamber. The track-pair capability in the actual chamber should be better by the ratio of sense-field spacings, i.e., (1.45/2) (1200) = 900 μ. Of course a reliable evaluation of the track-pair resolution awaits studies in dense hadronic jets.

C. Field Cage Design

The arrangement of wire planes in a jet cell is shown in Fig. 24. The jet cell consists of the grid-anode-grid sandwich, cathode wire planes on either side of it, field shaping wires at the inner and outer radii, which help minimize the end effects, and electrode surfaces attached to the inner Beryllium core and the outer aluminum skins. The cell is tilted with respect to the radial direction by slightly more than 15° as measured at the inner wire radius. This feature solves the left-right ambiguity, provides self-calibrating constraints from tracks which pass through cell-boundaries, and provides relatively uniform response for tracks at all azimuth. The cathode wires are graded in potential between about -5 kV and -15 kV in order to create a very uniform electric field throughout much of the cell volume. Potentials on the inner and outer guard wires and on the other electrode surfaces are shown to minimize the end effects. The resulting field is uniform within ± 0.1% over more than two-thirds of the cell. Potentials on the inner and outer HV "skins" are near -2 kV and -10 kV, respectively.

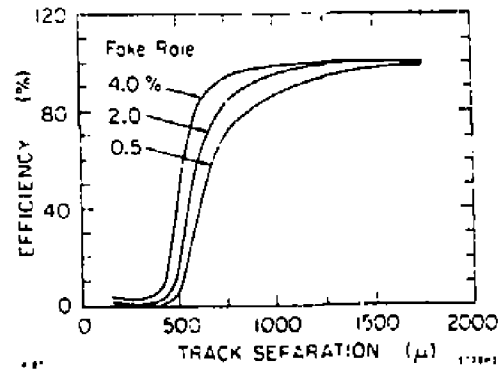

Fig. 23. Efficiency for detecting a second track as a function of its separation from the first.

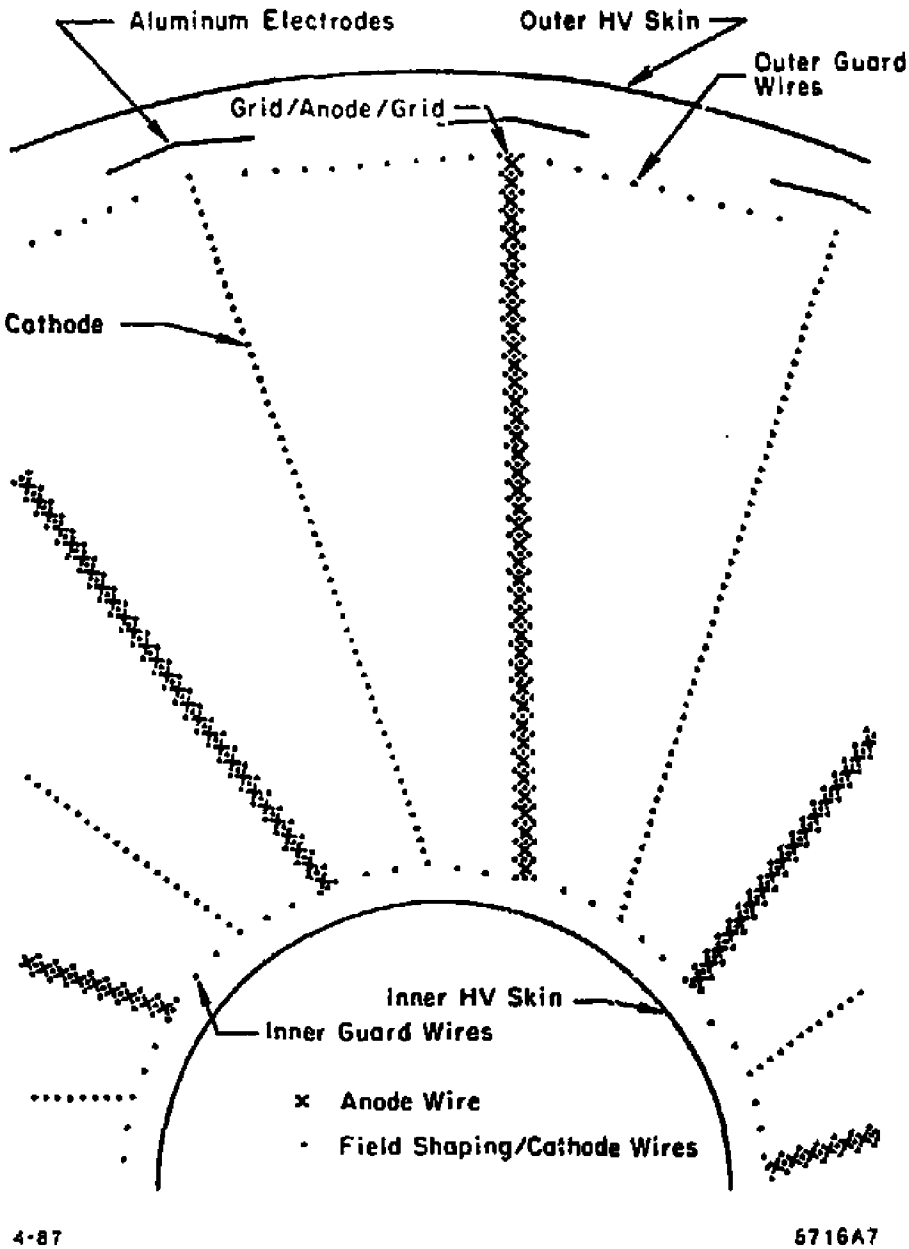

Fig. 24. Wire and electrode placement in the jet cells.

End effects are of course worst at the outer radius; to help minimize them ... minum electrodes are positioned over cathode and anode planes, and held ... -15 kV and -2 kV, respectively.

D. Mechanical Construction

To achieve good spatial accuracy in a drift chamber which utilizes a n... saturated drift velocity requires first a device which is mechanically and elect... statically stable, and second, a device which can be calibrated. Since the ... calibration of such a device requires accurate knowledge of the positions of each anode wire and to a lesser extent the cathode and grid wires too, we have adopted a technique for building the chamber which seeks to minimize the number of variables needed to characterize all the wire locations.

Wires are strung, a plane at a time, on very high precision grooved bars which locate the wires with an accuracy better than 3 μ. The entire plane of wires is attached to a ceramic foundation with epoxy, the wires "floating" ~ 100 μ above the ceramic, and captured in glue. Thus instead of dealing with the azimuthal and radial coordinates of each wire at each end of the chamber, we need to know only the two coordinates which fix the positions of the innermost and outermost wires in each plane.

The accuracy of the wire placement on the precision bars is shown in Fig. 25, where both optical and capacitive measurements have been used for the wire position measurements. The figure shows deviations from the expected wire positions in the wire plane. The wire positions are in general accurate to the 2 ... level, considerably better than is needed.

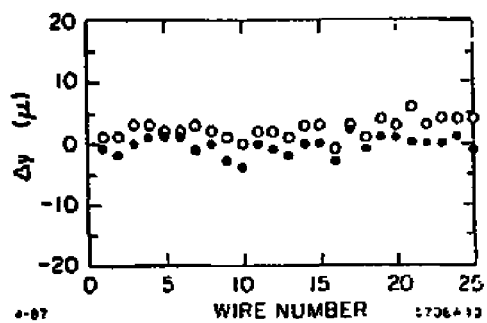

Fig. 25. Deviations of wires from their nominal positions in the plane of the wires. The open (closed) circles correspond to measurements made with a capacitive probe (optical microscope).

Fig. 26. Cathode plane assembly showing ceramic founcations, kapton circuitry, and pressure connector

The chamber construction is illustrated in Fig. 26. The jet cells are modular, made up of the ceramic foundation and wire planes mentioned above. They include flexible kapton printed circuits to bus all the signal and cathode wires past the positioning endplate and through a pressure feedthrough to amplifiers or high voltage resistor chains. These are mounted outside the chamber gas volume in order to isolate temperature generating components from the gas. A small mechanical mockup of one sector of the chamber is shown in Fig. 27. The anode wires are held on a small stainless steel foundation which butts against the endplate behind the ceramic foundations.

Kapton printed circuitry with factory installed kapton overlay has proved an effective way to bus large numbers of high voltage traces. The circuits typically

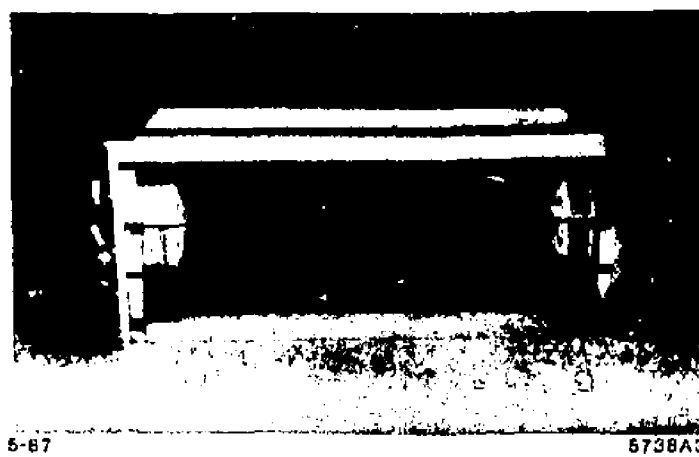

Fig. 27. Mechanical mockup of the DCVD showing two grid planes sandwiching the anode plane, guard wires, positioning endplates, and pressure connectors.

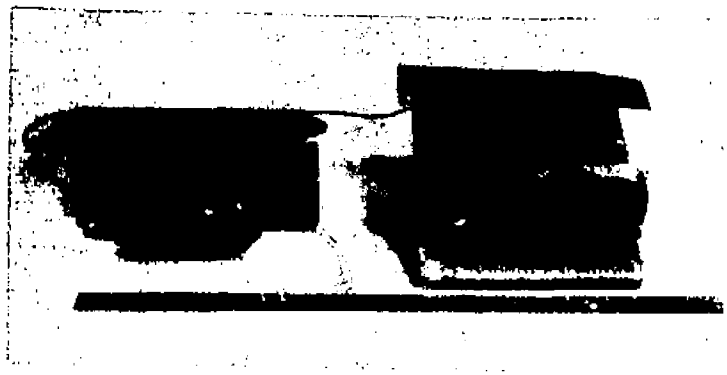

5-87 5738A30

Fig. 28. At left, multipin high voltage connector; at right, high voltage feedthrough consisting of kapton circuitry, potted into an aluminum pressure flange and connected to a high voltage connector.

have trace-to-trace resistances above 10^{13} Ω and can handle potential differences of several kilovolts across spacings of ~ 1 mm. Figure 28 shows the kapton circuitry and the pressure and high voltage connections. The high voltage connector holds off voltages of 10 kV between adjacent pins with leakage currents well below 1 nA. It can be run at voltages up to 16 kV with discharge rates well below 0.1 Hz.

Establishing the wire positions in the chamber is a two-part operation based on a system for reproducibly locating the ceramic foundations on smooth surfaces. Our system uses two "sockets" in each of the mating parts. The sockets are simply cylindrical pieces of steel into which a conical surface has been machined. (See Fig. 29.) When a precision ball bearing is captured between the mating sockets, and the sockets of one piece have been properly matched to those in the other, the parts will mate reproducibly to the micron level. A master template, also shown in the figure, defines the relationship between the pairs of sockets which fix the anode, cathode, and grid plane locations. Wire location proceeds as follows. First, the wire planes are accurately positioned with respect to the socket locations on the ceramic foundations and then secured in place with epoxy. This is accomplished using a large, high precision measuring microscope. Second, the ceramic foundations are transferred to the chamber endplates, where a pattern of mating sockets has been established by replicating the master template pattern ten times, once for each jet cell. This is done using a dividing head to fix the angle of rotation between one cell and the next. We hope to place wires in the chamber to within 10 μ of their nominal positions.

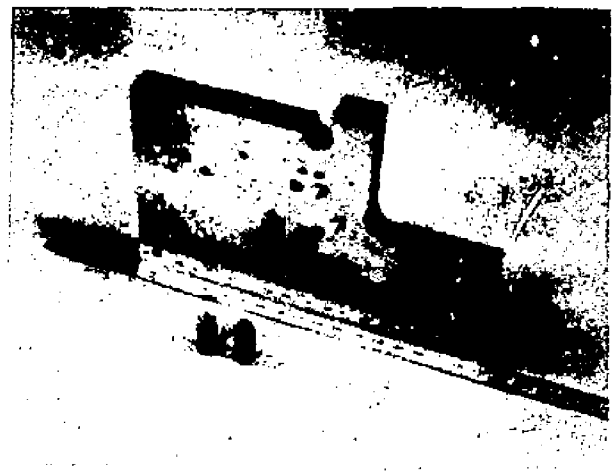

5-87 5738A29

Fig. 29. Master locating template, showing conical sockets and ball bearings.

One needs to understand wire positions in the chamber to the level of 5 to 10 μ to exploit fully the resolution inherent in the gas. This follows from the fact that the average resolutions per wire is about 30 μ, and roughly 12 wires will measure a common feature of the track, so the potential spatial precision will be about $30\mu/\sqrt{12} \sim 10\mu$.

E. Electronics

The readout electronics consists of a preamplifier mounted on the chamber, a postamplifier and shaper, and a wave form digitizing system. The sense wires, which are run at positive high voltage, couple capacitively through a 100 pF capacitor to a hybrid preamp designed by Radeka and Stefani.[18] It has a 3 ns rise time, 40 ns fall time, and a noise level of 150 μV, and is mounted directly outside the chamber gas volume. The preamp output is carried by about 15 feet of coax to a postamp mounted on the outside of the Mark II detector. It is similar in design to the postamp[19] developed for the Mark II Central Tracking Chamber, and includes shaping circuits to cancel the preamp fall time and the 1/t tail in the pulse. Its output runs via twisted pair to a modified version of the Mark II dE/dx flash-ADC module.[20] The new module incorporates a new fast memory chip, the Hitachi 10474-10, which extends the memory at 100 MHz to 10 μsec. The vertex detector FADC module is packaged 16 channels per single width Fastbus module, and uses a 6-bit flash ADC, the TRW-1029. The modules are read out with the SLAC Scanner Processor.[21]

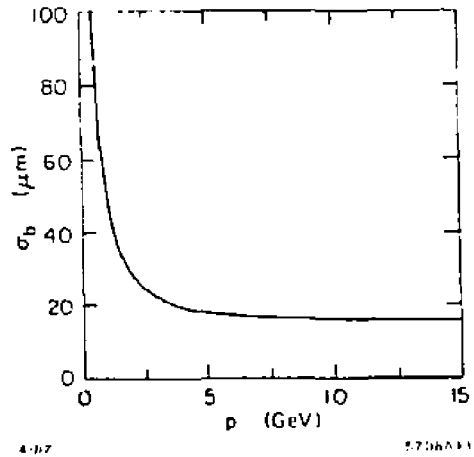

Fig. 30. Predicted impact parameter resolution as a function of track momentum.

F. Expected Performance

Figure 30 shows the impact parameter resolution of the new vertex detector used in conjunction with the Mark II central tracking chamber. The multiple scattering contribution is something worse than 60 μ/P (GeV/c), and the ultimate resolution at high momentum is about 15 μ. Studies of B-tagging at the SLC[72] show that roughly 33% of B decays can be cleanly tagged.

Hadronic jets from Z^0 decays are dense with charged particles, so adequate track-pair resolution is essential for successful vertex detection. One loses 10% of tracks when the angular segmentation is $\pm$ 10 mr which corresponds to a track-pair separation of $\pm$ 500 μ at the innermost radius of our chamber, r = 5 cm. As discussed above, the track-pair resolution achievable with our chamber is about 1000 μ. The fact that the jet cells are tilted effectively halves this number, however. In a chamber where the anode plane was radial, a given track could be obscured by tracks on either side of the anode plane which were collected slightly before the track in question. In a tilted cell (see Fig. 31), a track can be obscured by another track on the same side of the anode plane which has a slightly smaller drift time, but tracks which passed on the opposite side of the anode will appear to intersect the original track at sizable angles and obscure only a small part of it. Figure 31b shows the tracks which can be reconstructed after track-pair resolution effects are taken into account. A Monte Carlo simulation has shown that the B tagging efficiency in our chamber is about 10% lower than in a device with perfect track-pair resolution.

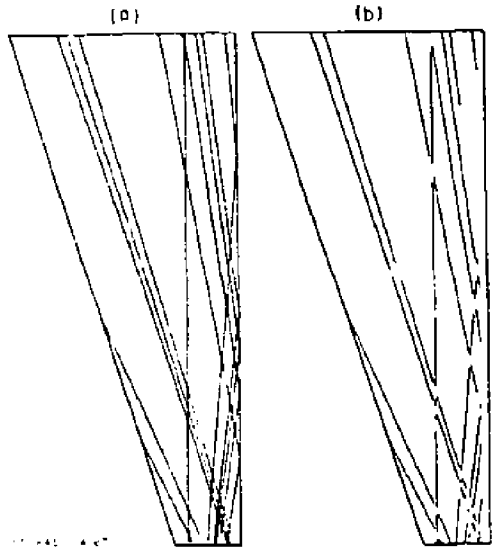

Fig. 31. Monte Carlo simulation of tracks passing through a jet cell with (a) perfect track-pair resolution; (b) 1500 μ track-pair resolution. See text for details.

IV. CONCLUSIONS

The art of detecting the decay vertices from heavy quarks and leptons is comparatively new at electron-positron storage rings. So far, drift chambers positioned just outside the vacuum pipes which surround the interaction region have provided the first accurate determinations of the tau and bottom lifetimes, and confirmed earlier measurements of charmed particle lifetimes. "Second generation" vertex detectors have demonstrated the feasibility of tagging heavy flavors by observing decay vertices, and are being used to search for anomalous decay topologies. These chambers have modest resolution on the scale of the effects they seek to measure, but are now well-understood and reliable tools.

A new generation of vertex detectors, considerably more ambitious, is under construction for experiments at SLC and LEP. They boast impact parameter resolution improved by a factor of four or more over previous detectors, and submillimeter track-pair resolution. The Mark II collaboration hopes to reach these goals with a high pressure precision drift chamber, and eventually surpass them with the addition of a silicon microstrip detector.

REFERENCES

1. G. J. Feldman *et al.*, Phys. Rev. Lett. **48**, 66 (1982).
2. E. Fernandez *et al.*, Phys. Rev. Lett. **51**, 1022 (1983).
3. See, for example, M. G. D. Gilchriese and D. M. Ritson in Proceedings of the 23rd International Conference on High Energy Physics, Berkeley, July 16 – 23, 1986.
4. A. Litke, in Proceedings of the International Conference on Advances in Experimental Methods for Colliding Beam Physics, Stanford, California, W. Kirk, editor, to be published in Nucl. Instr. and Meth.
5. J. A. Jaros, in Proceedings of the International Conference on Instrumentation for Colliding Beam Physics, Stanford, California, 1982, edited by W. Ash (SLAC Report No. 250).
6. D. Amidei, D. Baden, L. Gladney, L. Golding, J. Jaros, R. Ong, G. Trilling.
7. D. Amidei *et al.*, to be published in Phys. Rev. D. Preliminary results are given in J. A. Jaros, in Proceedings of the International Conference on Physics in Collision IV, Santa Cruz, California, Aug. 22 – 24, 1984, edited by A. Seiden, Editions Frontieres. First results were reported in J. A. Jaros *et al.*, Phys. Rev. Lett. **51**, 955 (1983).
8. L. Gladney *et al.*, Phys. Rev. D **34**, 2601 (1986).
9. J. C. Anjos *et al.*, Phys. Rev. Lett. **58**, 311 (1987).
10. N. S. Lockyer *et al.*, Phys. Rev. Lett. **51**, 1316 (1983).
11. J. A. Jaros, in Proceedings of the International Conference on Physics in Collision IV, Santa Cruz, California, August 22 – 24, 1984, edited by A. Seiden, Editions Frontieres.
12. See, for example, D. M. Ritson in Proceedings of the 23rd International Conference on High Energy Physics, Berkeley, July 16 – 23, 1986.
13. C. Wendt *et al.*, Phys. Rev. Lett. **58**, 1810 (1987).
14. R. Ong *et al.*, to be published in Phys. Rev. D.
15. J. Alexander, R. Dennis, P. Drell, W. Ford, R Fuzesy, R. Harr, K. Hayes, D. Hinshaw, C. Hoard, D. Hutchinson, J. Jaros, D. Koetke, S. Odaka, T. Ohama, R. Ong, M. Perl, J. Smith, G. Trilling, S. Wagner, P. Weber, S. White.
16. W. Farr *et al.*, Nucl. Instr. and Meth. **156**, 283 (1978).
17. J. Alexander *et al.*, Nucl. Instr. and Meth. **A252**, 350 (1986).

18. BNL Hybrid IO-354.

19. D. Briggs *et al.*, IEEE Trans. **NS-32**, 653 (1985).

20. D. Bernstein *et al.*, IEEE **NS-33**, 86 (1986).

21. H. Brafman *et al.*, IEEE Trans. **NS-32**, 336 (1985).

22. K. Hayes, Mark II/SLC Note #73 (unpublished internal memorandum).

DISCLAIMER